Slow Gold Adatom Diffusion on Graphene: Effect of Silicon Dioxide and Hexagonal Boron Nitride Substrates

Li Liu,[†,⊥] Zheyuan Chen,[†,⊥] Lei Wang,[‡] Elena Polyakova (Stolyarova),[†,¶] Takashi Taniguchi,[§] Kenji Watanabe,[§] James Hone,[‡] George W. Flynn,*[,†] and Louis E. Brus*[,†]

[†]Department of Chemistry and [‡]Department of Mechanical Engineering, Columbia University, New York, New York 10027, United States

[§]Advanced Materials Laboratory, National Institute for Materials Science, 1-1 Namiki, Tsukuba, 305-0044, Japan

Ⓢ Supporting Information

ABSTRACT: We examine the nucleation kinetics of Au clusters on graphene and explore the relationship with layer number and underlying supporting substrate of graphene. Using the mean field theory of diffusion-limited aggregation, morphology patterns are semiquantitatively analyzed to obtain Au adatom effective diffusion constants and activation energies. Under specified assumptions, the Au adatom diffusion constant for single-layer graphene supported on SiO_2 is ∼50 times smaller than that for hexagonal boron nitride (h-BN)-supported graphene and on the order of 800 times smaller than that for multilayer graphite. Bilayer graphene on SiO_2 shows a Au adatom diffusion constant similar to single-layer graphene on h-BN. Scanning probe data show that single-layer graphene is far flatter on h-BN than on SiO_2. Two factors are proposed as contributing to the observed lower diffusion constants on single-layer graphene: local surface roughness and homogeneous loss of dispersion/van der Waals electronic stability in multilayers. Graphene Raman spectroscopy shows little charge transfer between Au nanoparticles and graphene.
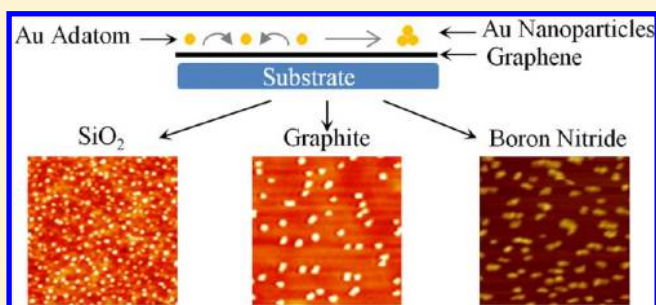
INTRODUCTION

Since its discovery in 2004, graphene has attracted massive research interest because of properties stemming from its unique electronic structure[1−4] and remarkably high crystallinity and strength.[5] Its 3D counterpart, graphite, is the smoothest of all substrates; molecules and nanocrystals adsorbed on its surface show extremely low friction and high mobility.[6−9] Graphite is composed of graphene sheets, which interact with neighboring ones through π-π stacking. Single-layer graphene, with each atom on the surface, shows a surface sensitivity to its surroundings, such as the underlying substrate. Several works[10−14] have studied the surface properties of graphene by examining the morphology of Au nanoparticles (NPs) formed by the diffusion of Au adatoms. In this work, we provide a deeper understanding of how the layer number and underlying supporting substrate determine the graphene surface properties. We find that the resulting kinetically controlled NP morphologies depend not only on the number of graphene layers through interlayer electronic stabilization but also on the surface roughness of the supporting substrate. Under the same deposition conditions, Au forms many well-dispersed, small NPs on single-layer (1L) graphene, but fewer and bigger NPs on graphite. By semiquantitatively analyzing the NP morphologies on these two substrates at saturation density, we find that the Au adatom effective diffusion constant is on the order of 800 times smaller for 1L graphene on SiO_2 than for graphite

surfaces. The Au adatom diffusion constant on 1L graphene mounted on h-BN is ∼50 times larger, approaching its value on the surface of bulk graphite. Thus, the NP growth kinetic process is effectively controlled by the nature of the substrate underneath the graphene. The present adatom diffusion study, in addition to previous studies of chemical reactivity,[15,16] charge transfer doping,[3,15,16] and electrical transport[17,18] show that, as a 2D material, graphene properties are strongly influenced by the local environment.

EXPERIMENTAL METHODS

Graphene samples were prepared by mechanical exfoliation of Kish graphite onto the SiO_2/Si substrates (thickness of SiO_2 ∼ 290 nm). The numbers of layers and structural integrity of graphene samples were characterized by Raman spectroscopy.[19] Vapor depositions of Au were carried out in an electron-beam (e-beam) evaporation chamber (SEMICORE SC2000) with a pressure of 5×10^{-7} Torr during deposition. The deposition substrates, which were kept around 19 °C during deposition, were about 1 m away from the Au source. Gold pellets with
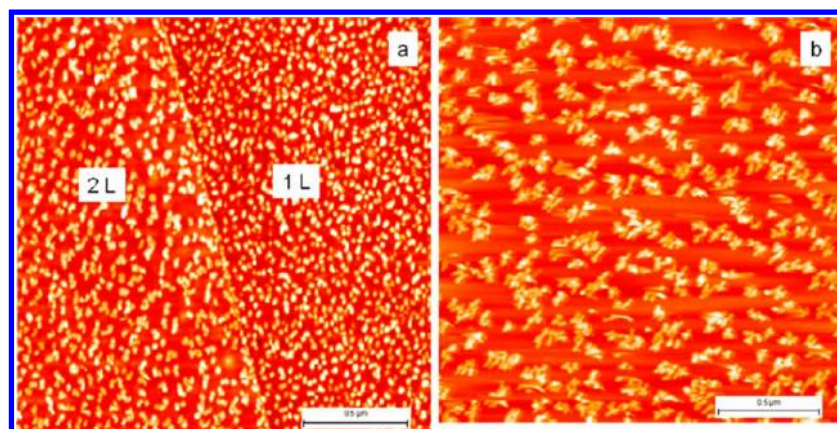
Figure 1. AFM images ($2 \times 2 \ \mu m^2$) of 5 Å Au deposited on single-layer (1L) and bilayer (2L) graphene (a) and graphite (b).
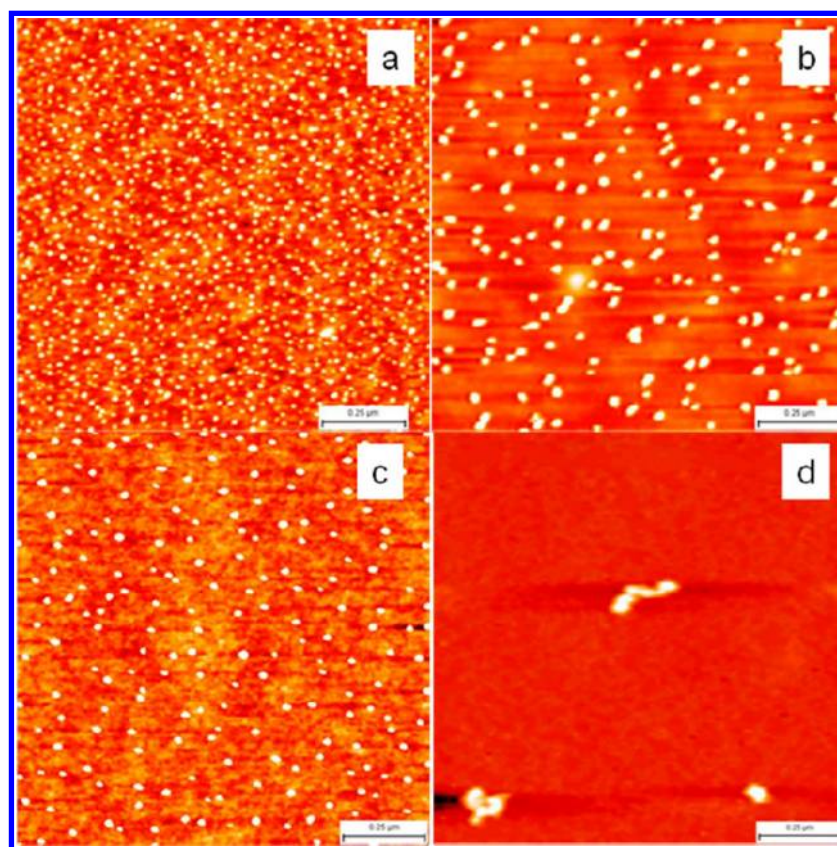

Figure 2. AFM images ($1 \times 1 \ \mu m^2$) of 1 Å Au deposited on 1L graphene (a) and graphite (b). After 2 h of thermal annealing at 350 °C, AFM images ($1 \times 1 \ \mu m^2$) on 1L graphene (c) and graphite (d).

99.999% purity (Kurt J. Lesker) were placed in a molybdenum boat (International Advanced Materials) and heated to near the melting temperature of gold using accelerated electron beams. Evaporation rates and Au dosages were monitored using a quartz crystal microbalance. For all the results shown in this paper, the evaporation rate was kept at 0.1 Å/s. Raman spectra of graphene and graphene with gold nanoparticles were performed in air at 25 °C using a confocal (40× objective) spectrometer with 600 grooves/mm grating. Ar-ion laser beam at 514.5 nm was focused to ~1 μm^2 in the sample plane, and low laser power (1 mW) was used to avoid any heating effects. The spectral resolution was around 8 cm^{-1}. Raman spectra were fitted with Voigt profiles to obtain peak widths. The "scotch tape" method[20] was adopted repetitively to prepare

graphene on h-BN substrates. BN flakes were first deposited onto SiO_2 using the "scotch tape" method. After removing the first piece of tape, a second piece of scotch tape with graphene flakes on it was put down on the substrate to deposit graphene onto the h-BN substrate. The presence of graphene was confirmed by atomic force microscope (AFM) and Raman spectroscopy as described in the Supporting Information.

■ RESULTS

As described in the previous section, Au was evaporated onto supported graphene at 19 °C in vacuum. The resulting NP AFM morphologies, observed for a 5 Å nominal (average thickness) Au coverage on 1L graphene, bilayer (2L) graphene, and graphite surfaces are shown in Figure.1. The graphene and
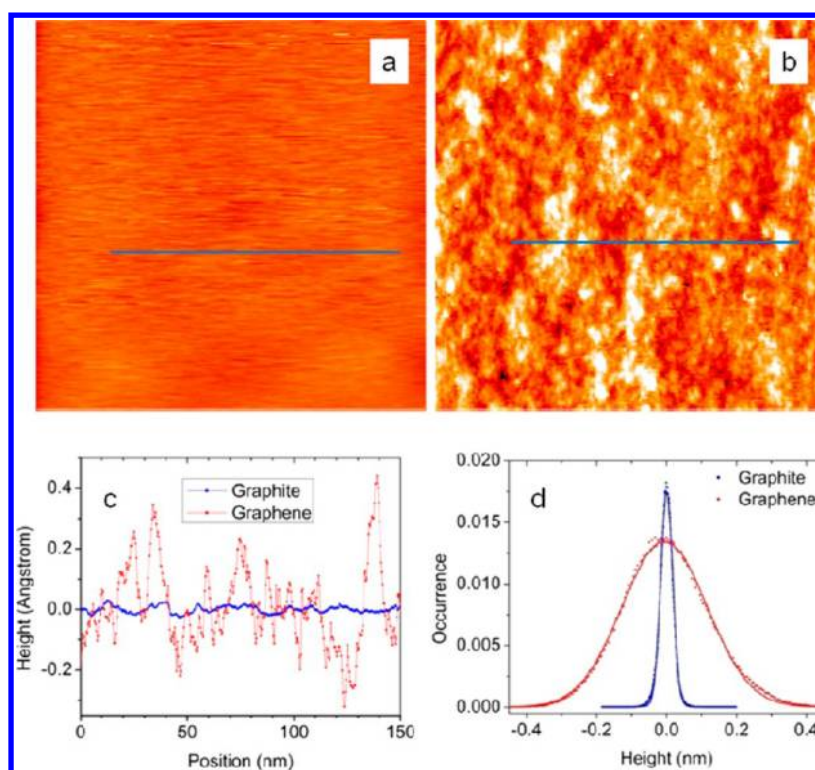
Figure 3. Large-scale STM images (200×200 nm^2) of graphite (a) and pristine 1L graphene (b). The images were obtained under ambient conditions in constant current mode. $V_{bias} = 0.5$ V and $I_{tunnel} = 0.5$ nA. (c) Line profiles along the blue lines shown in parts a and b. (d) Height distributions acquired from the whole areas of parts a and b. The histograms can be fitted with Gaussian functions with standard deviations of 17 and 121 pm for the graphite and pristine graphene surfaces.

graphite were on the same 1 cm^2 SiO$_2$/Si wafer chip, and the evaporated Au atom flux rate was essentially identical for both substrates. On the graphite surface, Au NPs coalesce to form ramified islands (Figure.1b), agreeing with previous results on air-cleaved highly ordered pyrolytic graphite (HOPG) examined via transmission electron microscope (TEM) in ultrahigh vacuum (UHV).[21] Because of the large Au−Au binding energy[22] ($\sim$3.8 eV), freely diffusing Au adatoms bind and form small compact NPs. These small NPs themselves diffuse somewhat more slowly and connect to each other to form islands, as occurs in the diffusion-limited aggregation (DLA) kinetic model.[23] Under the same deposition conditions, many well-dispersed, compact Au NPs are formed on the 1L graphene. On the 2L graphene, the formation of a few elbow-shaped Au NPs is seen, implying a transition of islands from an elongated shape to a ramified structure. The increased Au NP center-to-center distances observed in going from graphene to graphite indicates decreased Au adatom mobility on graphene. From these images, NP growth is far slower—and aggregation is far less extensive—on 1L graphene/SiO$_2$ than on graphite.

Prior studies[21,22,24] show Au adatoms are highly mobile on HOPG at 19 °C. Extreme mobility necessarily implies an extreme sensitivity to adsorbed contaminants as Au atoms explore large areas. The adsorbed gaseous impurities on air-cleaved HOPG could serve as extraneous nucleation centers, compared with clean vacuum-cleaved HOPG.[21] Under UHV conditions, it is necessary to either cleave HOPG in vacuum[21] or to anneal air-cleaved HOPG at 600 °C for several hours[24] to achieve the dendritic Au morphology characteristic of "clean" HOPG surfaces. Such extreme conditions are not used in this or previous graphene studies[10−14] of Au on graphene. Rather,

we explore Au kinetics under conditions more characteristic of graphene device fabrication. We observe substantial morphology differences on graphene and graphite under the same condition of residual contamination. In our experimental condition, coalescence and aggregation are extensive on graphite, but dendritic patterns are not observed. This suggests that we observe contamination-induced cluster nucleation on bulk graphite, similar to the previous air-cleaved HOPG studies. On 1L graphene, however, nucleation occurs far more readily for some intrinsic reason. On graphene, residual-contamination-induced nucleation is relatively less important.

Note also that polymeric tape residue from mechanical exfoliation is occasionally observed as "patchy" regions in AFM images (shown in the Supporting Information). Au adatoms tend to stick to the edges of tape residue "patchy regions" and nucleate. Graphene samples with "patchy regions" were discarded in our study.

At a lower (1 Å) Au dosage, the observed density of Au NPs is $\sim$1200 μm^{-2} (Figure 2a) on 1L graphene. After the sample was annealed at 350 °C in an Ar atmosphere for 2 h, the density of Au NPs dropped to $\sim$130 μm^{-2} (Figure 2c). On the graphite substrate, the density of Au NPs decreases from $\sim$180 μm^{-2} (Figure 2b) to $\sim$3 μm^{-2} (Figure 2d) after this annealing treatment. The observed density after annealing for the graphite sample agrees well with the average density of defect sites ($\sim$5 μm^{-2}) on bulk Kish graphite.[25,26] These sharp drops in the Au NP densities after thermal annealing confirm that the observed morphologies, formed here at 19 °C, are kinetically controlled. It is interesting to notice that the island density after annealing is similar to that of dendritic structures on "clean" HOPG,[21] suggesting that most of the adsorbed gaseous impurities may be
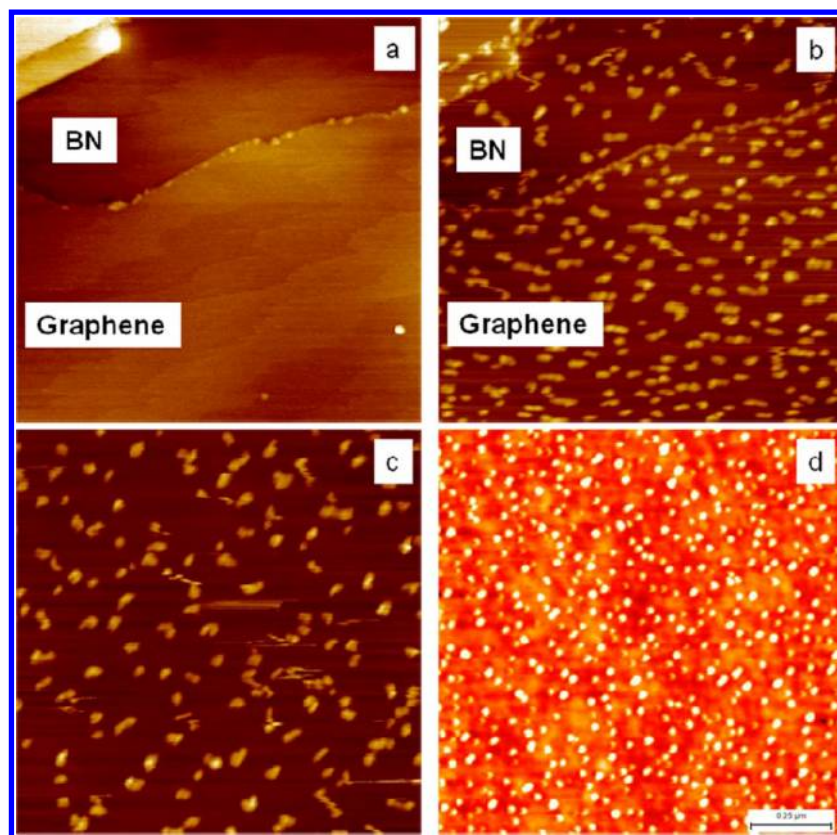
Figure 4. (a) AFM image ($1 \times 1 \ \mu m^2$) of pristine 1L graphene on hexagonal boron nitride (h-BN). (b) After deposition of 1 Å gold, AFM image ($1 \times 1 \ \mu m^2$) of Au NPs on 1L graphene supported by h-BN. (c) AFM image of Au NPs directly on h-BN. (d) AFM image of Au NPs on 2L graphene supported by SiO$_2$.

removed during the annealing process and have negligible effects on the diffusion of Au NPs.

To understand our nucleation data on graphene without "patchy" regions, we probed the morphology of unannealed samples using STM on a sample fabricated by the shadow mask method (see Supporting Information). Figure 3a and b shows large scale ($200 \times 200 \ nm^2$) STM images of graphite (HOPG) and 1L graphene on SiO$_2$. In contrast with the atomically flat graphite surface, the graphene surface displays many bright and dark features, which reflect the fact that graphene follows the locally high and low ("bumpy") features on the SiO$_2$ surface. Line profiles show height variations of ~0.05 Å and ~0.6 Å, respectively, for graphite and graphene surfaces over a 150 nm span (Figure 3c). The standard deviations of the height distributions for pristine 1L graphene and graphite are 121 and 17 pm, respectively (Figure 3d). The unannealed 1L graphene surface is 7 times rougher than flat graphite.

Our Au NP distributions are kinetically controlled, as discussed above. Luo et al.[10] studied the thermodynamic equilibrium properties of Au NPs on graphene after annealing at 400 °C. The graphene layer number dependence of the Au NP morphology was attributed to Coulombic interactions between charged Au NPs and graphene. We have explored possible charge transfer between graphene and Au NPs under the conditions of the present experiments using Raman spectroscopy. The graphene G Raman transition is known to shift and narrow with graphene charging.[27] We observe a negligible shift in G peak positions after evaporation of Au NPs, over a range of Au dosage, on SiO$_2$-supported graphene. The maximum G peak shift, 4 cm^{-1}, is actually achieved from deposition of a continuous bulk gold film of 100 Å thickness. A 4 cm^{-1} shift corresponds to a charge transfer doping of ~2.2×10^{12} cm^{-2} with a 191 meV Fermi energy shift,[28] as calibrated with top-gate graphene devices.[27] For 1 Å gold dosage onto graphene, the G peak shift due to Au NPs was less than 1 cm^{-1}. The G peak line width for this sample was observed to narrow by 2 cm^{-1}. This line width decrease corresponds to roughly ~4×10^{11} carriers/cm^{-2},[29] or about 5 holes per Au NP. This weak interaction is consistent with previously reported results.[28,30,31] Note also that DFT calculations have shown that charge transfer between graphene and very small gold clusters is less than $0.3e$ for each cluster.[32−37] Our graphene carrier density due to charge transfer, laterally averaged over the ~1 μm Raman spot size, is far below the density observed by Luo et al.[10] Under our conditions, there is little charge transfer between Au NPs and graphene.

NP growth kinetics at high adatom mobility can be markedly influenced by the existence of localized surface defects or traps. The morphology for 1L graphene in Figure 1 is actually very similar to those previously observed on bulk graphite surfaces where defect sites were intentionally generated by Ar ion bombardment.[38] Such defects trap mobile Au ad-atoms and act as nucleation centers. The surface diffusion activation energy for a gold atom, which sits in a graphene vacancy site, is measured to be ~2.5 eV.[39] The absence of the Raman D disorder band for graphene samples before and after Au deposition (see Supporting Information) implies that the density of such defects, individual C atoms with significant sp^3 hybridization, atom vacancy local defect sites, or both is very small.[19]

4308

dx.doi.org/10.1021/jp305521g | *J. Phys. Chem. B* 2013, 117, 4305–4312

We also studied Au NP kinetics for 1L graphene supported on hexagonal boron nitride (h-BN), a flat van der Waals layered material like graphite itself. Graphene is known to be substantially flatter, with more homogeneous electronic properties, on single-crystal h-BN than on SiO_2.[18,40,41] In Figure 4, 1L graphene on h-BN (bottom part of Figure 4a) shows almost the same AFM flatness (54 pm standard deviation in the height distribution) as does bulk h-BN itself (47 pm, upper part in Figure 4a). At the same AFM vertical resolution, graphene on SiO_2 in Figures 4b and Supporting Information S7 exhibits a rougher surface. Figure 4 shows the growth of Au NPs both for bare bulk h-BN and for 1L graphene on h-BN. On both these surfaces, NP growth is far faster than on 1L graphene supported on SiO_2. These data are quantitatively analyzed below.

■ DISCUSSION

Nonequilibrium NP growth kinetics can vary with the rate of adatom diffusion, with the rate of adatom deposition, F, per unit area and with the bonding strength between adatoms. Mean-field nucleation theory[42–44] has been extensively developed to interpret nonequilibrium NP formation on surfaces, and Zhou et al.[11] first suggested this approach for Au on graphene. We now discuss a semiquantitative application of the mean-field model.

As deposition time increases, there are three kinetic regimes: nucleation, transition from nucleation to growth, and steady-state growth. At the early stages of deposition, diffusing adatoms find each other and form stable nuclei (compact NPs). The number of nuclei increases with time, and eventually, newly deposited, diffusing adatoms predominately attach to preexisting nuclei. This creates a steady state regime in which nuclei continue to grow in size, but new nuclei are not created. At this nuclei saturation density, the mean free path of Au adatom diffusion, l, in nanometers, is equal to the mean Au NP separation.[44] In this kinetic process, Au adatom reevaporation might possibly occur;[45,46] however, we demonstrate in the Supporting Information section that gold atoms condense completely on graphene and graphite surfaces; that is, the effect of reevaporation is negligible in our experiments.

At 5 Å coverage, we see the effect of NP diffusion: NPs form ramified islands (see Figure 1b). At 1 Å coverage (see Figure 2), we observe mostly the individual NP with few aggregates; this is the steady-state kinetic regime discussed above. Au adatoms will have far larger diffusion constants than Au NPs, and adatom diffusion dominates the kinetics in this regime. Venables theoretically considered the effect of mobile NPs on the steady-state saturation NP density and concluded that this effect is significant only at the highest temperatures and lowest arrival rates.[47] Brune has also argued that even dimer cluster diffusion plays a minor role in determining the final NP density.[44] Hence, we tentatively neglect the motion of a few atom clusters and larger NPs in the growth kinetics. With this simplification, the Au NP saturation density, n, is predicted to be[43]

$$n(Z) \sim N_0 \eta(Z) \left(\frac{F}{N_0 \nu} \right)^{i/(i+2.5)} \exp\left[\frac{E_i + iE_d}{(i + 2.5)kT} \right] \quad (1)$$

as described more fully in the Supporting Information section. Here, Z is the substrate area coverage by NPs (unitless); Z thus depends upon the total deposition time. N_0 is the substrate atomic density (cm^{-2}); $\eta(Z)$ is a dimensionless calculated parameter; F is the flux rate of arriving atoms ($cm^{-2}\ s^{-1}$); ν is an

effective surface vibration frequency ($\sim 10^{11} - 10^{13}\ s^{-1}$); i is the number of Au atoms in the critical cluster; E_i is the Au atom binding energy in the critical cluster; and finally, E_d is the diffusion activation energy of a single Au atom.

The critical cluster of size i is the most unstable cluster in thermodynamic nucleation theory.[43] Clusters of size smaller than i decay rapidly, and their density can be expressed in a Walton relation derived from "detailed balance" thermodynamic equilibrium.[48] Clusters larger than size i grow and form the stable NPs shown in the AFM images. The critical cluster can be large if the adatom bonding is weak, as occurs in rare gas aggregation on graphite. However, DFT calculations show that bonds between gold atoms are strong (~ 3 eV) in clusters of size up to 7.[34] This is close to the cohesive energy of bulk gold and larger than the estimated adsorption energy of gold adatoms on graphene (~ 0.45 eV).[49] Au clusters are expected to be stable at room temperature;[50] therefore, the critical size i should be small, and in Figure 5, we consider both $i = 1$ and 2. For $i = 1$, n simplifies to

$$n(Z) \sim N_0 \eta(Z) \left(\frac{F}{N_0 \nu} \right)^{1/3.5} \exp\left(\frac{E_d}{3.5kT} \right) \quad (2)$$
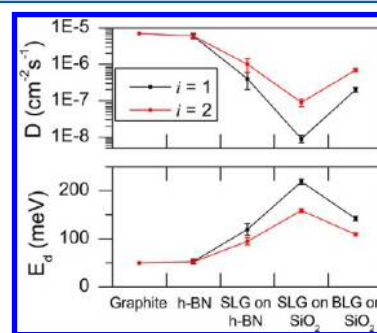

Figure 5. The calculated diffusion energy, E_d, and diffusion constant, D, of Au adatoms on various surfaces (graphite, h-BN, 1L graphene (SLG) on h-BN, SLG on SiO_2, and 2L graphene (BLG) on SiO_2) with the corresponding uncertainties, obtained from the relative ratio of the Au cluster density, n. Calculations using different critical sizes i are given in black ($i = 1$) and red ($i = 2$) curves for comparison. The density, n, is normalized to the same flux rate (0.005 monolayer/s). For graphite, E_d and D are assumed as 50 meV and $7 \times 10^{-6}\ cm^{-2}\ s^{-1}$, independent of critical size i. The diffusion constant, D, is given to only 1 significant figure in view of the many approximations.

In this model, the thermally activated Au adatom diffusion constant is $D = (a^2 \nu_d / 4)e^{-E_d/kT}$. Here, a is the atomic spacing distance on graphene. Thus, at low NP coverage, Z, we see that the NP saturation density is proportional to $(F/D)^{1/3.5}$. At steady state, the higher flux, F, increases the NP density, and faster adatom diffusion decreases the NP density. However, this dependence is relatively weak, to the 0.286 power. To increase the NP density by an order of magnitude at constant flux, D must decrease by a factor of ~ 3200, for example. If we compare densities on 1L graphene, n_{1L}, and bulk graphite, n_∞, at the same flux, F, we have

$$n_{1L}/n_\infty = [D_\infty/D_1]^{1/3.5} \quad (3)$$

At 1 Å coverage, we observe NP densities of 1200 and 180 μm^{-2} on 1L graphene and graphite, respectively. On 1L graphene, the Au NP densities at 2 and 3 Å coverage are 930 and 880 μm^{-2}, respectively. The close Au NP densities at 1

(1200 μm^{-2}), 2, and 3 Å coverage indicate that Au NPs reach their saturation density at a coverage of 1 Å on graphene substrates. On graphite surfaces, the Au cluster density (180 μm^{-2}) at 1 Å is very close to what was obtained from a previous study on a highly oriented pyrolitic graphite (HOPG) surface,[24] which was conducted at a higher F. Under the present conditions, Au NPs essentially reach saturation density on both 1L graphene and graphite.

Equation 3 is a semiquantitative result in view of the approximations and uncertainties. It indicates that the effective Au adatom diffusion constant, D, decreases by roughly 3 orders of magnitude on graphene/SiO$_2$ compared with graphite. The diffusion constant difference may be even more than 3 orders of magnitude as a result of the effect of residual contamination on graphite nucleation. The diffusion constant on bulk graphite can be estimated from a recent calculation of the Au adatom diffusion activation energy, E_d = 50 meV.[49] If we take the attempt frequency, ν_d, to be 10^{12} s^{-1} and the atomic jump length, a, to be the C−C bond length (0.14 nm) considering that the most stable position of the Au atom is vertically on top of a carbon atom,[12,35,49] we can estimate the graphite diffusion constant, $(a^2\nu_d/4)e^{-E_d/kT} = 7 \times 10^{-6}$ cm^{-2} s^{-1}. Using this value, we obtain estimates for D for Au on other surfaces using eq 3. The results are shown in Figure 5.

How should we interpret this vastly smaller diffusion constant for Au atoms on graphene compared with graphite? First, adatom diffusion is known to be affected by the surface strains[51−54] that occur on many bulk materials and layered thin films.[55] Within a certain range, a compressive strain tends to reduce the adatom diffusion energy, and tensile strain tends to increase it, as shown in a STM study of Ag adatom diffusion on bulk Ag (111) and pseudomorphic 1 ML Ag/Pt (111) surfaces.[56] The diffusion activation energies of Ag adatoms on these fcc (111) surfaces are the energy differences between the hollow sites and the bridge sites. These energies increase under tensile strain but decrease under compressive strain.[57] Strain also exists on curved surfaces such as carbon nanotubes (CNTs) and molecular sieves. A positive curvature on the outer surface of a CNT applies tensile strain and increases the adatom diffusion activation energy.[58] In general, to make this curvature idea quantitative, one needs to understand the interaction between the adatom and the substrate.

In its free-standing suspended state, 1L graphene displays mesoscopic ripples with an estimated ~1 nm height variation that span ≤25 nm laterally.[59] In contrast, 1L graphene on mica is as flat as bulk graphite.[60] When supported and annealed at 400 °C on SiO$_2$/Si substrates, graphene follows the local SiO$_2$ roughness such that the graphene−SiO$_2$ van der Waals interaction energy is balanced by the elastic deformation energy of graphene, as revealed by an AFM study.[61] A scanning tunneling microscopy study has shown that thermal annealing increases the roughness of graphene surfaces,[16] apparently by making graphene more conformal with the rough SiO$_2$ supporting substrate. Yet even our unannealed 1L samples are 8 times rougher than bulk graphite, as shown above.

On this rough graphene surface, there will be regions of both concave and convex curvature. These local regions will have different Au atom diffusion constants. In a sense, the diffusion constant will be patchy, not homogeneous across the surface, as is the case for bulk graphite. Regions with a smaller diffusion constant will slow the motion of Au adatoms and locally tend to enhance nucleation compared with defect-free graphite. Nanometer-sized regions of very slow diffusion act as a type

of "defect" in NP growth kinetic theory. Thus, the 1L graphene diffusion constant, D, in Figure 5 should be considered an effective value, incorporating such local variations in D. In addition, inhomogeneous electric fields from the silicon dioxide affect graphene physical properties. Fields such as these create spatially varying electron−hole puddles occurring in 1L graphene on SiO$_2$.[62] These disorder-induced fluctuations of electron or hole carrier density are ~10^{12} cm^{-2} in magnitude and vary on a lateral 30 nm length scale. Similarly, local inhomogeneous electric fields cause the bilayer graphene band gap, created in devices by external field effect gating, to vary strongly from spot to spot.[11] Our present results show that Au NP nucleation kinetics is also a sensitive way to probe this lateral patchiness in graphene physical properties.

What substrate-related forces act upon diffusing Au atoms? Neutral Au atoms are polarizable and, thus, are attracted to regions of high electric field. The previously discussed inhomogeneous SiO$_2$ electric fields partially penetrate through 1L and 2L graphene. Both vertical and horizontal inhomogeneous fields exist above the graphene surface and can act directly on the Au adatoms; however, an order-of-magnitude estimate indicates this direct interaction is far too weak to influence 19 °C thermal diffusion.

We suggest the strongest force acting upon Au adatoms is incipient bonding with graphene. A Au atom has one valence electron, and thus, we might compare its chemistry with that of the H atom. Actually, free H atoms deposited on bulk graphite form a weak ~0.7 eV covalent bond to one C atom,[63−65] which distorts out-of-plane in a manner similar to the Au case.[66] Calculation shows a diffusion activation energy on the order of 1 eV; thus, diffusion of H on graphene should be very slow at 19 °C.[67] This H atom interaction with the graphite basal plane has also been studied for 1L and 2L graphene on SiO$_2$, for which it was found that that 1L was about a factor of 15 more reactive than 2L.[13] A similar experimental result, that the 1L graphene basal plane on SiO$_2$ is significantly more reactive than bulk graphite, is also observed for graphene oxidation by O$_2$ at elevated temperatures[15,16] and for diazonium bonding at 19 °C.[68] Recent study[69] shows that methyl radical binds to graphite in a way similar to how H does. The methyl radicals bound to graphite on one C atom become mobile (start to diffuse) near room temperature, which suggests that the diffusion barrier is related to the weak chemical bonding to one C atom. A DFT calculation shows that C binding to bilayer is the same strength as the binding to monolayer. But generally speaking, DFT theory does not correctly take into account the strong dispersion/van der Waals type interactions that exist between the semimetallic graphene sheets and between graphene and Au substrates.[70−72] Experimentally, as discussed above, multilayer graphenes are less reactive for basal plane attack.

If the diffusion activation barrier increases as the bonding strength and C atom distortion increase, then we can understand how Au adatoms would have a far lower diffusion constant on 1L graphene than on bulk graphite. In principle, this slow diffusion has both homogeneous and roughness-related inhomogeneous contributions. We observe that diffusion on 2L graphene occurs at an intermediate rate; 2L graphene is more stable than 1L graphene due to the π bonding between the layers, and in addition, the 2L material shows less roughness. Both factors should create weaker Au bonding and, thus, faster diffusion.

In Figure 5, there are three cases in which the surface is relatively flat: bulk h-BN, bulk graphite, and 1L graphene on h-BN. Diffusion on flat h-BN is almost as fast as on graphite: $D = 6 \times 10^{-6}$ cm^{-2} s^{-1} on h-BN compared with 7×10^{-6} cm^{-2} s^{-1} on graphite, and this value is not sensitive to the choice of critical size, i. Thus, the semimetallic nature of graphite versus the insulating nature of h-BN does not make a significant difference in the incipient interaction with adsorbed Au.

The case of 1L graphene on h-BN is quite interesting. Diffusion of Au atoms on 1L graphene mounted on h-BN is fast with respect to diffusion on 1L graphene adsorbed on a SiO$_2$ substrate. However, D is a factor of ~13 smaller when compared with pure h-BN, and a factor of ~15 lower when compared with bare graphite, assuming critical size i equal to 1. We suggest that the lower Au diffusion constant for flat 1L graphene on h-BN, compared with pure graphite, is in part due to the homogeneous loss of interlayer stabilization: 1L graphene deposited on h-BN is not in crystalline registry with the substrate. The azimuthal angle is not controlled in deposition, and the planar hexagonal unit cells are somewhat different in size. The dispersion/van der Waals stabilization of 1L graphene on h-BN should be less than on graphite. By comparing 1L graphene on h-BN and SiO$_2$, the effect of roughness causes an ~100 meV increase in the diffusion energy barrier. Furthermore, the effect of homogeneous stabilization is estimated as ~70 meV from the comparison of graphite and 1L graphene on h-BN. Note also that the diffusion energy for Au adatoms on 2L graphene mounted on a SiO$_2$ surface is close to that of 1L graphene on h-BN. As the critical size, i, increases from 1 to 2, the diffusion constants, D, of Au NPs increases to different extents on each substrate in Figure 5. The increase in D leads to an expected decrease in the diffusion barriers E_d. The general trend still holds, even though the difference of both D and E_d decreases between various substrates.

We observe a far lower saturation density for Au NPs on a h-BN substrate (see Figure 4c) as compared with a SiO$_2$ substrate. In addition, the NPs on h-BN are larger than those on SiO$_2$. From the AFM height histograms, the average NP height increases from 2.3 to 3.1 nm (see Supporting Information Figure S6) when the underlying substrate is changed from SiO$_2$ to h-BN. The coverage of Au NPs on SiO$_2$ (30%) is 50% larger than that on h-BN (20%). Despite this large increase in coverage by Au NPs, the total calculated volume of Au NPs per unit area is essentially independent of the substrate. Thus, graphene accommodates the Au atom kinetic energy of deposition quite well; all incident Au atoms appear to be captured. This is also consistent with the deposition of gold atoms in the complete condensation regime, as argued in the Supporting Information section.

CONCLUSION

We semiquantitatively analyze the morphology of Au NPs appearing in AFM images using nucleation theory. Two factors, local roughness and homogeneous interlayer stabilization, appear to effect the diffusion of Au ad-atoms on 1L graphene supported on various substrates. Incipient chemical bonding of Au atoms to graphene appears to be the main interaction affecting diffusion. Raman spectroscopy indicates negligible charge transfer between Au NPs and graphene. The adatom diffusion activation energy has been estimated to be on the order of 100 meV. The high sensitivity of the graphene surface to the underlying substrate may be used to control the size and morphology of metal nanoparticles on graphene for applica-

tions in catalysis and in sensor development. The substrate sensitivity we observe for Au nucleation kinetics on graphene is an example of the "molecular" nature of graphene: physical properties depend upon the local environment.

ASSOCIATED CONTENT

Ⓢ Supporting Information

Experimental methods, AFM images of Au NPs on contaminated graphene, Raman spectra, and height and diameter histograms of Au NPs are provided. The equation to calculate the saturation density of Au NPs is also discussed. This information is available free of charge via the Internet at http://pubs.acs.org.

AUTHOR INFORMATION

Corresponding Author
*E-mails: (G.W.F.) gwf1@columbia.edu, (L.E.B.) leb26@columbia.edu.

Present Addresses
∥Department of Chemistry, Texas A&M University, College Station, TX 77843.
¶Graphene Laboratories Inc., 79 Richmond Blvd 1-A, Ronkonkoma, NY 11779.

Author Contributions
⊥These authors contributed equally to this work.

Notes
The authors declare no competing financial interest.

REFERENCES

(1) Novoselov, K. S.; Geim, A. K.; Morozov, S. V.; Jiang, D.; Zhang, Y.; Dubonos, S. V.; Grigorieva, I. V.; Firsov, A. A. Science 2004, 306, 666−669.
(2) Berger, C.; Song, Z. M.; Li, T. B.; Li, X. B.; Ogbazghi, A. Y.; Feng, R.; Dai, Z. T.; Marchenkov, A. N.; Conrad, E. H.; First, P. N.; et al. J. Phys. Chem. B 2004, 108, 19912−19916.
(3) Novoselov, K. S.; Geim, A. K.; Morozov, S. V.; Jiang, D.; Katsnelson, M. I.; Grigorieva, I. V.; Dubonos, S. V.; Firsov, A. A. Nature 2005, 438, 197−200.
(4) Zhang, Y. B.; Tan, Y. W.; Stormer, H. L.; Kim, P. Nature 2005, 438, 201−204.
(5) Lee, C.; Wei, X. D.; Kysar, J. W.; Hone, J. Science 2008, 321, 385−388.
(6) Bardotti, L.; Jensen, P.; Hoareau, A.; Treilleux, M.; Cabaud, B. Phys. Rev. Lett. 1995, 74, 4694−4697.
(7) Ge, G. L.; Brus, L. J. Phys. Chem. B 2000, 104, 9573−9575.
(8) Ge, G. L.; Brus, L. E. Nano Lett. 2001, 1, 219−222.
(9) Tang, J.; Ge, G. L.; Brus, L. E. J. Phys. Chem. B 2002, 106, 5653−5658.

(10) Luo, Z. T.; Somers, L. A.; Dan, Y. P.; Ly, T.; Kybert, N. J.; Mele, E. J.; Johnson, A. T. C. *Nano Lett.* **2010**, *10*, 777−781.

(11) Zhou, H. Q.; Qiu, C. Y.; Liu, Z.; Yang, H. C.; Hu, L. J.; Liu, J.; Yang, H. F.; Gu, C. Z.; Sun, L. F. *J. Am. Chem. Soc.* **2010**, *132*, 944−946.

(12) Zhou, H. Q.; Yu, F.; Yang, H. C.; Chen, M. J.; Wang, G.; Sun, L. F. *Chem. Phys. Lett.* **2011**, *518*, 76−80.

(13) Pandey, P. A.; Bell, G. R.; Rourke, J. P.; Sanchez, A. M.; Elkin, M. D.; Hickey, B. J.; Wilson, N. R. *Small* **2011**, *7*, 3202−3210.

(14) Barreiro, A.; Rurali, R.; Hernandez, E. R.; Bachtold, A. *Small* **2011**, *7*, 775−780.

(15) Liu, L.; Ryu, S. M.; Tomasik, M. R.; Stolyarova, E.; Jung, N.; Hybertsen, M. S.; Steigerwald, M. L.; Brus, L. E.; Flynn, G. W. *Nano Lett.* **2008**, *8*, 1965−1970.

(16) Ryu, S.; Liu, L.; Berciaud, S.; Yu, Y. J.; Liu, H. T.; Kim, P.; Flynn, G. W.; Brus, L. E. *Nano Lett.* **2010**, *10*, 4944−4951.

(17) Morozov, S. V.; Novoselov, K. S.; Schedin, F.; Jiang, D.; Firsov, A. A.; Geim, A. K. *Phys. Rev. B* **2005**, *72*, 201401.

(18) Dean, C. R.; Young, A. F.; Meric, I.; Lee, C.; Wang, L.; Sorgenfrei, S.; Watanabe, K.; Taniguchi, T.; Kim, P.; Shepard, K. L.; et al. *Nat. Nanotechnol.* **2010**, *5*, 722−726.

(19) Casiraghi, C.; Pisana, S.; Novoselov, K. S.; Geim, A. K.; Ferrari, A. C. *Appl. Phys. Lett.* **2007**, *91*, 233108.

(20) Novoselov, K. S.; Jiang, D.; Schedin, F.; Booth, T. J.; Khotkevich, V. V.; Morozov, S. V.; Geim, A. K. *Proc. Natl. Acad. Sci. U.S.A.* **2005**, *102*, 10451−10453.

(21) Darby, T. P.; Wayman, C. M. *J. Cryst. Growth* **1975**, *28*, 41−52.

(22) Darby, T. P.; Wayman, C. M. *J. Cryst. Growth* **1975**, *29*, 98−108.

(23) Witten, T. A.; Sander, L. M. *Phys. Rev. Lett.* **1981**, *47*, 1400−1403.

(24) Anton, R.; Schneidereit, I. *Phys. Rev. B* **1998**, *58*, 13874−13881.

(25) Yang, R. T.; Wong, C. *J. Chem. Phys.* **1981**, *75*, 4471−4476.

(26) Evans, E. L.; Griffiths, R. J. M.; Thomas, J. M. *Science* **1971**, *171*, 174−175.

(27) Das, A.; Pisana, S.; Chakraborty, B.; Piscanec, S.; Saha, S. K.; Waghmare, U. V.; Novoselov, K. S.; Krishnamurthy, H. R.; Geim, A. K.; Ferrari, A. C.; et al. *Nat. Nanotechnol.* **2008**, *3*, 210−215.

(28) Giovannetti, G.; Khomyakov, P. A.; Brocks, G.; Karpan, V. M.; van den Brink, J.; Kelly, P. J. *Phys. Rev. Lett.* **2008**, *101*, 026803.

(29) Berciaud, S.; Ryu, S.; Brus, L. E.; Heinz, T. F. *Nano Lett.* **2009**, *9*, 346−352.

(30) Entani, S.; Sakai, S.; Matsumoto, Y.; Naramoto, H.; Hao, T.; Maeda, Y. *J. Phys. Chem. C* **2010**, *114*, 20042−20048.

(31) Shikin, A. M.; Prudnikova, G. V.; Adamchuk, V. K.; Moresco, F.; Rieder, K. H. *Phys. Rev. B* **2000**, *62*, 13202−13208.

(32) Yazyev, O. V.; Pasquarello, A. *Phys. Rev. B* **2010**, *82*, 045407.

(33) Amft, M.; Sanyal, B.; Eriksson, O.; Skorodumova, N. V. *J. Phys.: Condens Matter* **2011**, *23*, 205301.

(34) Wang, G. M.; BelBruno, J. J.; Kenny, S. D.; Smith, R. *Phys. Rev. B* **2004**, *69*, 195412.

(35) Varns, R.; Strange, P. *J. Phys.: Condens. Matter* **2008**, *20*, 225005.

(36) Carara, S. S.; Batista, R. J. C.; Chacham, H. *Phys. Rev. B* **2009**, *80*, 115435.

(37) Subrahmanyam, K. S.; Manna, A. K.; Pati, S. K.; Rao, C. N. R. *Chem. Phys. Lett.* **2010**, *497*, 70−75.

(38) Lopez-Salido, I.; Lim, D. C.; Dietsche, R.; Bertram, N.; Kim, Y. D. *J. Phys. Chem. B* **2006**, *110*, 1128−1136.

(39) Gan, Y. J.; Sun, L. T.; Banhart, F. *Small* **2008**, *4*, 587−591.

(40) Xue, J.; Sanchez-Yamagishi, J.; Bulmash, D.; Jacquod, P.; Deshpande, A.; Watanabe, K.; Taniguchi, T.; Jarillo-Herrero, P.; LeRoy, B. J. *Nat. Mater.* **2011**, *10*, 282−285.

(41) Novoselov, K. S.; Dubonos, S. V.; Morozov, S. V.; Hill, E. W.; Grigorieva, I. V.; Geim, A. K. *J. Low Temp. Phys.* **2005**, *139*, 65−72.

(42) Brune, H.; Roder, H.; Boragno, C.; Kern, K. *Phys. Rev. Lett.* **1994**, *73*, 1955−1958.

(43) Venables, J. A.; Spiller, G. D. T.; Hanbucken, M. *Rep. Prog. Phys.* **1984**, *47*, 399−459.

(44) Brune, H. *Surf. Sci. Rep.* **1998**, *31*, 121−229.

(45) Arthur, J. R.; Cho, A. Y. *Surf. Sci.* **1973**, *36*, 641−660.

(46) Jensen, P.; Larralde, H.; Pimpinelli, A. *Phys. Rev. B* **1997**, *55*, 2556−2569.

(47) Venables, J. A. *Philos. Mag.* **1973**, *27*, 697−738.

(48) Walton, D. *J. Chem. Phys.* **1962**, *37*, 2182−2188.

(49) Jensen, P.; Blase, X.; Ordejon, P. *Surf. Sci.* **2004**, *564*, 173−178.

(50) Smith, R.; Nock, C.; Kenny, S. D.; Belbruno, J. J.; Di Vece, M.; Palomba, S.; Palmer, R. E. *Phys. Rev. B* **2006**, *73*, 125429.

(51) Barth, J. V.; Brune, H.; Ertl, G.; Behm, R. J. *Phys. Rev. B* **1990**, *42*, 9307−9318.

(52) Brune, H.; Roder, H.; Boragno, C.; Kern, K. *Phys. Rev. B* **1994**, *49*, 2997−3000.

(53) Frank, F. C.; Vandermerwe, J. H. *Proc. R. Soc. London, Ser. A* **1949**, *198*, 205−216.

(54) Needs, R. J.; Godfrey, M. J.; Mansfield, M. *Surf. Sci.* **1991**, *242*, 215−221.

(55) Vandermerwe, J. H.; Tonsing, D. L.; Stoop, P. M. *Surf. Sci.* **1994**, *312*, 387−398.

(56) Brune, H.; Bromann, K.; Roder, H.; Kern, K.; Jacobsen, J.; Stoltze, P.; Jacobsen, K.; Norskov, J. *Phys. Rev. B* **1995**, *52*, 14380−14383.

(57) Ratsch, C.; Seitsonen, A. P.; Scheffler, M. *Phys. Rev. B* **1997**, *55*, 6750−6753.

(58) Shu, D. J.; Gong, X. G. *J. Chem. Phys.* **2001**, *114*, 10922−10926.

(59) Meyer, J. C.; Geim, A. K.; Katsnelson, M. I.; Novoselov, K. S.; Booth, T. J.; Roth, S. *Nature* **2007**, *446*, 60−63.

(60) Lui, C. H.; Liu, L.; Mak, K. F.; Flynn, G. W.; Heinz, T. F. *Nature* **2009**, *462*, 339−341.

(61) Ishigami, M.; Chen, J. H.; Cullen, W. G.; Fuhrer, M. S.; Williams, E. D. *Nano Lett.* **2007**, *7*, 1643−1648.

(62) Martin, J.; Akerman, N.; Ulbricht, G.; Lohmann, T.; Smet, J. H.; Von Klitzing, K.; Yacoby, A. *Nat. Phys.* **2008**, *4*, 144−148.

(63) Jeloaica, L.; Sidis, V. *Chem. Phys. Lett.* **1999**, *300*, 157−162.

(64) Sha, X. W.; Jackson, B. *Surf. Sci.* **2002**, *496*, 318−330.

(65) Hornekaer, L.; Sljivancanin, Z.; Xu, W.; Otero, R.; Rauls, E.; Stensgaard, I.; Laegsgaard, E.; Hammer, B.; Besenbacher, F. *Phys. Rev. Lett.* **2006**, *96*, 156104.

(66) Amft, M.; Lebegue, S.; Eriksson, O.; Skorodumova, N. V. *J. Phys.: Condens. Matter* **2011**, *23*, 395001.

(67) Yang, M.; Nurbawono, A.; Zhang, C.; Wu, R.; Feng, Y.; Ariando. *AIP Adv.* **2011**, *1*, 032109.

(68) Sharma, R.; Baik, J. H.; Perera, C. J.; Strano, M. S. *Nano Lett.* **2010**, *10*, 398−405.

(69) Mandeltort, L.; Choudhury, P.; Johnson, J. K.; Yates, J. T. *J. Phys. Chem. Lett.* **2012**, *3*, 1680−1683.

(70) Sarabadani, J.; Naji, A.; Asgari, R.; Podgornik, R. *Phys. Rev. B* **2011**, *84*, 155407.

(71) Sernelius, B. E. *Phys. Rev. B* **2012**, *85*, 195427.

(72) Lebedeva, I. V.; Knizhnik, A. A.; Popov, A. M.; Lozovik, Y. E.; Potapkin, B. V. *Phys. Chem. Chem. Phys.* **2011**, *13*, 5687−5695.